

Predicting sit-to-stand adaptations due to muscle strength deficits and assistance trajectories to complement them

Vinay Kumar^{1,*}, Takahide Yoshiike², and Tomohiro Shibata^{1,*}

¹ Department of Human Intelligence Systems, Graduate School of Life Science and Systems Engineering, Kyushu Institute of Technology, Kitakyushu, Japan

² Honda R&D Co., Ltd., Saitama, Japan

Correspondence*:

Vinay Kumar
vinaym815@gmail.com

Tomohiro Shibata

tom@brain.kyutech.ac.jp

2 ABSTRACT

3 Sit-to-stand (STS) transition is one of the most bio-mechanically challenging task necessary
4 for performing activities of daily life. With muscle strength being the most dominant, many co-
5 occurring factors influence how individuals perform STS. This study investigates the STS changes
6 and STS failure caused by strength deficits using the trajectories generated employing an open-
7 loop single shooting optimization framework and musculoskeletal models. The strength deficits
8 were introduced by simultaneously scaling the maximum isometric strength of muscles in steps
9 of 20%. The optimization framework could generate successful STS transition for models with up
10 to 60% strength deficits. The joint angle kinematics, muscle activation patterns, and the ground
11 reaction forces from the 0% strength deficit STS transition match those observed experimentally
12 for a healthy adult in literature. Comparison of different strength deficit STS trajectories shows
13 that when the vasti muscle gets saturated, the activation of the antagonistic hamstring muscle
14 reduces to relieve it, which then saturates the gluteus maximus muscle. Subsequently, the
15 hamstring deactivation observation and motion tracking results are used to suggest the vasti
16 muscle weakness to be responsible for STS failure. Finally, in this study, the successful STS
17 trajectory of the 80% strength deficit model assisted externally at the torso are presented to
18 demonstrate the optimization framework's capability to synthesize assisted STS transition. The
19 trajectory features utilization of external assistance as and when needed to complement strength
20 deficits for successful STS transition. Our results will help plan intervention and design novel STS
21 assistance devices.

22 **Keywords:** Sit-To-Stand, Musculoskeletal Model, Strength Deficit, Single Shooting Optimization, Open Loop Controller, Assist-A-
23 Needed

1 INTRODUCTION

24 Sit-to-stand (STS) transition is a precursor to walking, hence critical for performing daily life activities
25 and an independent lifestyle. Lower extremity strength plays an important role in human STS, and its
26 deficits are thought to limit the STS functionality. Studies have shown that the lower extremity strength is a
27 strong predictor of the ability of older adults to perform STS from the lowest possible chair height (Hughes
28 et al., 1996; Schenkman et al., 1996). However, the decline in muscle strength often co-occurs with other
29 physiological and psychological impediments such as reduced balance, joint pain, and depression, making
30 it difficult to access its independent effect on STS using experiments (Lord et al., 2002). Also, besides
31 subject-specific factors, STS is influenced by many extrinsic factors like foot placement, knee position, and
32 chair height, making the process of designing and conducting experiments complex.

33 Some past studies have used STS trajectories generated using optimization and musculoskeletal models
34 to avoid the complications of experiments. Pandy et al. (1995) presented a cost function that generates STS
35 trajectories with similar muscle activations to those of experiments. Bobbert et al. (2016) and Yokota et al.
36 (2016) searched for trajectories that reduced loads on the muscles and the knee joint. However, the studies
37 mentioned above have made either minimal or no observations about STS changes caused by strength
38 deficits. Further, these studies have also not investigated how strength deficits might lead to unsuccessful
39 STS.

40 Many older individuals incapable of independent STS transition can perform the same when aided
41 externally. This external assistance can help maintain or recover lower extremity strength when provided
42 in an assist-as-needed manner. Thus it is desirable to generate reference assistance trajectories that assist
43 as and when needed and by the amount that is needed. Mombaur and Hoang (2017) and Geravand et al.
44 (2017) have used optimization to discover assistance trajectories that support part of the user's weight
45 during STS and squat-to-stand motions, respectively. However, both the studies use human models with
46 independently torque actuated joints. The hamstrings and the rectus femoris are two biarticular muscles
47 that play an essential role in the STS transition. Their biarticularity couples the torques produced at the hip
48 and knee joints. This coupling should not be ignored, especially when generating reference STS assistance
49 trajectories, as it may lead to assistance profiles that over actuates one of these muscles, leading to muscle
50 contracture and eventually lower back issues. The coupling is also crucial for accurately investigating the
51 STS changes and the STS failure caused by the strength deficits.

52 This study aims to identify the STS changes and the STS failure caused by muscle strength deficits
53 and the external assistance trajectories that can complement them for successful STS transition. Towards
54 these aims, first, the single shooting optimization framework used to generate the STS trajectories for
55 musculoskeletal models with varying degrees of strength deficit and the methods used to analyze them are
56 presented. Subsequently, for validation, the joint angle trajectories, the muscle activation patterns, and the
57 ground and seat reaction forces from the STS trajectory of the 0% strength deficit model are contrasted
58 against those observed experimentally for a healthy adult in literature. Then, the different strength deficit
59 trajectories are compared to observe the changes in STS caused by strength deficits. Afterwards, the
60 STS failure is investigated using the motion-tracking results. Finally, the successful STS trajectory of an
61 externally assisted musculoskeletal model, incapable of performing unaided STS transition, is presented
62 to demonstrate the optimization framework's ability to generate externally assisted STS trajectory. The
63 findings of this study will help plan intervention and design novel STS assistance devices that operate in an
64 assist-as-needed manner.

65 Within the single shooting optimization framework, we have parameterized the open-loop excitation
66 trajectories of the actuators similarly to Pandy et al. (1995), and Yokota et al. (2016). The excitation
67 trajectories are used to integrate the system's equation of motion of the equation forward in time to
68 generate the resultant motion. Then the cost function evaluated on the resultant motion is used to tune the
69 actuator's excitation trajectories. Another possible optimization framework's structure is where the joint
70 angle trajectories are parameterized. The tuning of joint angle trajectories in these frameworks is based on
71 the solutions of inverse dynamics in the case of skeletal models and the solutions of inverse dynamics and
72 static optimization in the case of musculoskeletal models. Such frameworks are used for STS synthesis
73 in Sadeghi et al. (2013); Norman-Gerum and McPhee (2018); Yang and Ozsoy (2020), to discover STS
74 trajectories with minimum actuator efforts in Yoshioka et al. (2007, 2012), and to predict the unilateral
75 grab-rail assisted STS trajectories of a virtually unhealthy adult in Yang and Ozsoy (2021); Ozsoy and Yang
76 (2021). Direct collocation is another potential optimization framework and performs optimization over
77 both the joint angle and the actuator excitation trajectories Bobbert et al. (2016). We selected open-loop
78 single shooting trajectory optimization for its straightforward implementation and effortless extension to
79 incorporate closed-loop controllers in future works.

80 It is difficult to identify and detail all of the parameters that shape the STS trajectories generated
81 using optimization. For example, Bobbert et al. (2016), and Yokota et al. (2016) does not contain
82 information about the initial guesses to the optimization algorithm, while Pandy et al. (1995) does
83 not include information about the mechanical limits used to restrict the motion to the physiologically
84 plausible range. Therefore we have made all the source code and results from this study public at
85 <https://github.com/ShibataLab/PredictiveSTS>.

2 METHODS

86 An overview of the single shooting optimization framework used to generate STS trajectories in this
87 study is shown in Figure 1. The optimization framework tunes the values of decision variables using the
88 aCMA-ES algorithm (Arnold and Hansen, 2010). aCMA-ES is a stochastic gradient-free optimization
89 algorithm that adapts a Gaussian distribution towards low energy regions. It was selected for its enhanced
90 robustness to locally optimal solutions than the gradient-based algorithms. At each generation, aCMA-ES
91 samples a batch of candidate solutions from the Gaussian distribution being adapted. Subsequently, the
92 cost function values are evaluated for all the candidates after running the respective forward simulations.
93 aCMA-ES then adapts the Gaussian distribution based on the cost function values and proceeds to the next
94 generation and so on until one of the stopping criteria is met.

95 In subsection 2.1, the musculoskeletal models used to generate STS trajectories with the optimization
96 framework are detailed. Subsection 2.2 includes the details of the decision variables and the termination
97 criteria used with the optimization framework, while subsection 2.3 describes the cost function. Subsection
98 2.4 includes a summary of the motion-tracking setup used to investigate STS failure. The final subsection,
99 i.e., 2.5 details the process used to prepare the experimental data against whom the STS trajectory of the
100 0% strength deficit model is validated.

101 2.1 Musculoskeletal Model

102 Musculoskeletal models with different strength deficits for this study were obtained by simultaneously
103 scaling the maximum isometric strengths of the muscles present within the base model. The base model,
104 also shown in Figure 2, is a simplified version of the LaiArnold2017 model (Lai et al., 2017). The

105 LaiArnold2017 model represents an average-sized adult male of mass $75Kg$ and height $170cm$. The base
106 model is two-dimensional with eight hill-type muscles and three degrees of freedom, while the source
107 model is 3D with 80 hill type muscles and 37 degrees of freedom. The simplifications were needed to
108 make the optimization problem computationally tractable. The following paragraph detail some of these
109 simplifications.

110 From the LaiArnold2017 model, the left leg and the associated muscles were removed. The masses of
111 arms, forearms, hands and the head were lumped to the torso's center of mass (COM). The mass and
112 inertia of the torso after lumping were halved to account for the missing left leg and the associated muscles.
113 The right foot was fixed to the ground using a weld joint. Then the degrees of freedom corresponding
114 to the sagittal plane motion of the ankle, knee, hip and lumbar joints were added. The 0° angle of the
115 hip, knee, ankle and lumbar joints corresponds model standing upright. From 0° , the positive joint angles
116 correspond to ankle dorsiflexion, knee flexion, hip flexion, and lumbar extension; and the negative joint
117 angles correspond to the opposite. The lumbar joint was locked to -10° , for reasons explained in subsection
118 2.5 and thus, the model effectively has three degrees of freedom. The lower extremity muscles with similar
119 functions were combined to single muscle-tendon units as realized in Ong et al. (2019). Figure 2 shows
120 insertion points and the paths of the resultant muscles included in the base model, i.e., gluteus maximus
121 (GMAX), biarticular hamstrings (HAMS), iliopsoas (ILPSO), biarticular rectus femoris (RF), vasti (VAS),
122 biarticular gastrocnemius (GAS), soleus (SOL), and tibialis anterior (TA). Table 1 lists the maximum
123 isometric strengths for the muscles included in the base model along with the acronyms. At the beginning
124 of simulation, the muscle states were set by equilibrating the muscle-tendon units with the default activation
125 of 0.05.

126 The chair-body contact interactions were modelled using a point on point kinematic constraint between
127 the femur head and the chair. During simulation, the kinematic constraint was disabled if the vertical
128 reaction forces required to maintain it turned non-compressive or satisfied the slipping condition. The seat
129 kinematic constraint, once disabled, could not be re-engaged and thus prevented optimization from getting
130 stuck into local optima with multiple chair rises. The model had nonlinear torsional springs representing
131 ligaments at the hip, knee, and ankle joints, limiting the motion to physiologically plausible ranges. They
132 generated torques when the hip joint flex beyond 120° or extends below 30° , or the knee joint flex beyond
133 140° or extend beyond 0° , or the ankle dorsiflex beyond 30° or plantarflex beyond 40° . These ranges
134 are from the LaiArnold2017 model, and the other parameters of the torsional springs are from Ong et al.
135 (2019).

136 External assistance was introduced at the torso's COM in the musculoskeletal model that failed to perform
137 unassisted STS transition. The rationale behind introducing it at the torso is explained in subsection 3.3. The
138 external assistance was modelled using two independent point forces acting in the vertical and horizontal
139 directions for implementation simplicity. Their respective magnitudes were limited to the 0-200 N range.
140 Before computing actuation, the excitation signals to point forces were passed through first-order activation
141 dynamics. The first-order activation dynamics (Millard, 1999) is the same as those of the hill-type muscle
142 present within the musculoskeletal models and had a time constant of 0.1 sec. It reduced the optimization
143 framework's sensitivity to individual assistance force decision variables by making the external assistance
144 trajectories smoothers. The OpenSim API (Delp et al., 2007) was used to formulate the musculoskeletal
145 model's equation of motion and their forward integration.

146 **2.2 Optimization Setup**

147 Our optimization framework tuned the values of nodes points obtained by discretizing the excitation
 148 trajectories of the actuators present within the musculoskeletal model and the STS duration (t_f). Piecewise
 149 linear functions with a fixed time difference of 0.1 sec between consecutive nodes were used for this
 150 discretization. The upper limit for simulation duration (t_{max}) was selected to be 1.6 sec, similar to
 151 Yokota et al. (2016). All the musculoskeletal models had 8 hill-type muscles, and the externally assisted
 152 musculoskeletal model had two additional point actuators. At t_0 , the actuators had their default activation.
 153 Thus, the optimization problem had 129 decision variables when generating unassisted STS trajectories
 154 and 161 decision variables when generating assisted STS trajectories.

155 As mentioned before, aCMA-ES is a stochastic gradient-free optimization algorithm that adapts a
 156 Gaussian distribution towards low energy regions. The actuator excitation values corresponding to the
 157 model sitting in a chair were used for the initial guess for the mean of the Gaussian. The algorithm was
 158 restarted if the number of generations exceeded 4000 or if the improvement in the cost values was lower
 159 than 1.0 for the best candidate solutions over the immediate 250 generations. At each restart, the generation
 160 counter and the covariance matrix were reset to default, and the mean was set to the been-seen candidate
 161 solution till then. Four restarts were performed to account for the stochasticity and the non-linearity
 162 optimization space before selecting the candidate solution with the lowest cost as the optimal trajectory.
 163 We used the *libcmaes* library (CMA-ES, 2013) for the aCMA-ES algorithm.

164 **2.3 Cost Function**

165 The cost function we selected to engender STS transition is a linear combination of ten different terms
 166 and can be expressed as follows:

$$\phi_{total} = \sum_{i=1}^{10} w_i \phi_i \quad (1)$$

167 where w_i is the relative weight of i^{th} cost term, i.e., ϕ_i . The mathematical expressions of the ten cost
 168 terms are given in Equations 2 - 12. Please refer to Table 2 for the list of symbols used in these equations.
 169 All the elements associated with different costs were computed in SI units.

$$\phi_1 = \frac{d(C_f, C_{goal})}{d(C_0, C_{goal})} \quad (2)$$

$$\phi_2 = [1 - \alpha] \int_{t_0}^{t_f} \frac{e^{t/\tau}}{\tau[e^{t_f/\tau} - 1]} F_{chair,y}(t) dt \quad (3)$$

$$\phi_3 = \sqrt{\frac{\sum_i \int_{t_0}^{t_f} a_i(t)^2 dt}{\sum i}} \quad (4)$$

$$\phi_4 = \sqrt{\frac{\sum_i \int_{t_0}^{t_f} \dot{a}_i(t)^2 dt}{\sum i}} \quad (5)$$

$$\phi_5 = \int_{t_0}^{t_f} ||F_{Assist}(t)|| dt \quad (6)$$

$$\phi_6 = \sum_n \int_{t_0}^{t_f} |T_{n,limit}(t)| dt \quad (7)$$

$$\phi_7 = \alpha \max_{\{t_0, t_f\}} (0, |F_{feet,x}(t)| - \mu F_{feet,y}(t)) \quad (8)$$

$$\phi_8 = \alpha \max_{\{t_0, t_f\}} |ZMP_x(t) - Feet_x(t)| dt \quad (9)$$

$$\phi_9 = \alpha [|\dot{\theta}_{hip}(t_f)| + |\dot{\theta}_{knee}(t_f)| + |\dot{\theta}_{ankle}(t_f)|] \quad (10)$$

$$\phi_{10} = \alpha \left[\begin{array}{l} \max_{\{t_{SR}, t_f\}} (F_{feet,y}(t)) - mg \\ \min_{\{t_{SR}, t_f\}} (F_{feet,y}(t)) - mg \\ |(F_{feet,y}(t_f)) - mg| \end{array} \right] \quad (11)$$

$$\alpha = 1 - \frac{\min(d(C_f, C_{goal}), d(C_0, C_{goal}))}{d(C_0, C_{goal})} \quad (12)$$

170 Cost ϕ_1 is the ratio of euclidean distances between the goal and t_f COM positions, and the goal and t_0
 171 COM positions. The goal COM position corresponds to the model standing upright. Cost ϕ_2 penalizes the
 172 model staying in contact with the chair. Cost ϕ_2 features an increasing exponential and thus penalizes the
 173 chair contact interactions more during the later of STS than prior. Costs ϕ_3 and ϕ_4 penalize the control
 174 effort and its rate of change, respectively. Cost ϕ_5 demotivates excessive use of external assistance. It was
 175 set to zero for the unassisted STS trajectories. Cost ϕ_6 discourages hyper-flexion and hyper-extension
 176 of joints. Costs ϕ_7 and ϕ_8 respectively penalize the feet contact forces that would lead to slip or tipping
 177 over the heel or toes. Cost ϕ_9 penalizes the body motion at t_f while cost ϕ_{10} penalizes the excessive body
 178 accelerations.

179 The scalar α represents STS progress and is illustrated in Figure 3. While learning successful STS, the
 180 optimization first comes across unstable STS trajectories. Costs ϕ_7 to ϕ_{10} are scaled by α to prevent them
 181 from hindering the exploration of unstable STS trajectories for stable ones. The evolution of different
 182 costs and their relative contributions to the total cost for the best candidate solutions observed during the
 183 synthesis of unassisted STS trajectory using 0% strength deficit model is illustrated in Figure 4. During the
 184 initial generations, the COM position at t_f is far away from standing posture COM, hence the value of α is
 185 closer to zero. Then as the optimization progresses, cost ϕ_2 moves the model out chair and cost ϕ_1 moves
 186 it towards standing posture. This moves C_f towards C_{goal} , and the value of α and so the contribution costs
 187 ϕ_7 to ϕ_{10} increases. As the model learns to stand up, an increasing amount of control effort is required
 188 and thus, the relative contributions of costs ϕ_3 and ϕ_4 increase with optimization progress. The values of
 189 relative weights associated with different costs, i.e., w_i , were determined by trial and error and listed in
 190 Table 3 along with other cost function related hyperparameters. Figure S1 of the supplementary material
 191 shows the generated STS trajectories are reasonably robust to the w_i values.

192 2.4 Motion Tracking Setup

193 The OpenSim CMC tool-based motion tracking was used to investigate the failure of STS in this study.
 194 The CMC tool computes the actuator excitation levels at user-specified time intervals that will drive the

195 generalized coordinates (\vec{q}) of the musculoskeletal model towards a desired kinematic trajectory (\vec{q}_{exp}) in
 196 the presence of external forces. At any given time t , the CMC tool first computes the desired acceleration
 197 $\ddot{\vec{q}}^*$ using the following proportional derivative control law:

$$\ddot{\vec{q}}^*(t + T) = \ddot{\vec{q}}_{\text{exp}}(t + T) + \vec{k}_v [\dot{\vec{q}}_{\text{exp}}(t) - \dot{\vec{q}}(t)] + \vec{k}_p [\vec{q}_{\text{exp}}(t) - \vec{q}(t)] \quad (13)$$

198 where, \vec{k}_v and \vec{k}_p are the feedback gains on the velocity and position errors, respectively. Since the
 199 forces that muscles apply cannot change instantaneously, the desired accelerations are computed some
 200 small-time T in the future. Then, CMC tool uses static optimization to distribute the load across synergistic
 201 actuators using static optimization. CMC tool offers two formulations for static optimization referred to as
 202 slow target and fast target. We used the fast target formulation. It minimizes the sum of squared controls
 203 augmented by a set of equality constraints which can be mathematically represented as follows:

$$J = \sum_{i=1} e_i^2 \quad (14)$$

$$C_j = \ddot{q}_j^* - \ddot{q}_j \quad \forall j \quad (15)$$

204 where e_i is the control input/excitation of i^{th} actuator at time t and q_j is the j^{th} generalized coordinate.
 205 Since for many \ddot{q}_j^* the muscles might not be able to produce sufficient forces, usually ideal torque actuators
 206 are added to the musculoskeletal model to prevent the fast target formulation from failing. Usually, the
 207 forces/torques produced per unit control effort for the ideal actuators is much lower than muscles. In
 208 such setups, following Equation 14, ideal torque actuators produce significant force/torque only when the
 209 muscles are saturated, and hence they are also referred to as reserve actuators. Since the CMC tool does not
 210 support event detection based disabling of constraints, the seat contact force was supplied as an external
 211 force rather than a kinematic constraint. The seat force was pre-computed for the target STS trajectory
 212 before running the CMC tool.

213 2.5 Experimental Data Processing

214 We have used the experimental data recordings, which also forms the basis of Lao et al. (2019) and Lao
 215 et al. (2020), to validate the optimal STS trajectory generated using the 0% strength deficit model. The
 216 experimental data contains optical marker trajectories, surface EMG signals and the ground and seat-pan
 217 reaction forces for 12 healthy adult subjects performing assisted and unassisted STS. Since the experimental
 218 data does not contain the functional trials needed for musculoskeletal model scaling, we have used the
 219 recording of only a single subject with weight and height closest to our model. The selected subject weighs
 220 71Kg and is 169cm tall. The source musculoskeletal model represents an adult male of mass 75Kg and
 221 height 170cm.

222 The unassisted STS trajectories has 6 trials under four conditions, i.e., arms folded across chest, arms
 223 hanging freely next to the body, natural STS, and slow pace imitating assisted STS. We used the 18 trials
 224 belonging to the first three categories. The optical markers were fixed to the musculoskeletal model on the
 225 average marker positions of the T-pose trial. This musculoskeletal model with registered optical markers
 226 was used for inverse kinematics. We defined the beginning and the end of STS as the times when hip
 227 flexion and hip extensions velocities smoothed with a rolling window of 0.1s were respectively higher

228 or lower than $20^\circ/s$. The resulting joint trajectories from the 18 trials are shown in Figure S2. The mean
229 initial posture observed in experiments is compared to the initial posture used to generate STS trajectories
230 in Figure 5. As can be observed, the simulation model was moved slightly forward towards the feet, and the
231 lumbar joint was locked to -10° . The adjustments were made to compensate for the non-actuated lumbar
232 joint. Also, the simulation's initial posture is easier to stand up from due to the torso lying closer to the feet.

233 The sEMG signals were processed by first passing through a fourth-order Butterworth bandpass filter
234 of 10Hz and 350Hz cutoff frequencies. Then they were rectified and subsequently passed through a
235 fourth-order Butterworth lowpass filter of 3Hz cutoff frequency. Finally, the sEMG signals were normalized
236 using the peak values present in the maximum voluntary control trials. The ground and seat reaction force
237 trajectories were not processed. Figures S3 and S4 respectively illustrate the sEMG and ground and seat
238 reaction force trajectories from the 18 trails used in this study.

3 RESULTS

239 The optimization could generate successful STS trajectories for the 0%, 20%, 40% and 60% strength
240 deficit models. However, for the 80% strength deficit model, the optimization framework could generate
241 successful STS trajectories only when the model was assisted externally. We refer to the STS trajectories
242 as the model's trajectories for conciseness, even though the models were only a single component of the
243 optimization framework. The STS trajectories are divided into the three phases suggested in Millington
244 et al. (1992) to facilitate discussions. Phase 1 starts with the trunk flexion and ends when the model loses
245 contact with the chair. Phase 2 starts with the knee extension and ends when the hip joint is maximally
246 flexed. Phase 3 begins with the reversal of trunk flexion to extension and ends with the model standing
247 upright. The vertical black dotted lines in Figures 6-12 marks the transition between the three phases.

248 The results are organized into three subsections. In subsection 3.1 the kinematics and dynamics of
249 the 0% strength deficit model's STS trajectory are discussed and contrasted against the experimental
250 observations. In subsection 3.2, first, the adaptations caused by muscle strength deficits are reported, and
251 then an explanation for the optimization's failure to generate STS using the 80% strength deficit model
252 is suggested. In subsection 3.3, the features of the STS trajectory generated using the externally assisted
253 80% strength deficit model are discussed. Please refer to Figures 6-11 and Table 4 during the following
254 subsections for details. The resultant joint torques, in Figure 11 and Table 4, were obtained using inverse
255 dynamical analysis of the STS trajectories. During inverse dynamical analysis, the muscles forces were
256 excluded, while the seat constraint and assistance forces were supplied as external forces. The resultant
257 joint torques and the contributions of muscles to them were computed using the OpenSim (Delp et al.,
258 2007).

259 3.1 Unassisted STS Trajectory of 0% Strength Deficit Model

260 The joint angle, the muscle excitation, the COM position and velocity, feet force zero moment point
261 (*ZMP*), and the contact force trajectories associated with the 0% strength deficit model's STS trajectory
262 are respectively illustrated in Figures 6 to 10. The STS motion is initiated by activating the ILPSO and
263 RF muscles (Figure 7). Their activation generates torque around the hip joint and flexes the torso forward
264 (Figure 11). It is followed by the deactivation of ILPSO and RF muscles and gradually increasing activations
265 of the GMAX and HAMS muscles. Due to the trunk's forward flexion, the COM's horizontal velocity
266 increases and peaks (Figure 8) before the activations of the GMAX and HAMS muscles increase to control
267 the torso's forward flexion. Also, the activation of VAS muscle increases to prepare for seat-off. Phase 1

268 ends when the VAS muscle has generated sufficient torques around the knee joint to lift the musculoskeletal
269 model off the chair. The seat off takes place with the body's COM lying behind feet force ZMP (Figure 9).
270 During phase 2, the GMAX and HAMS muscle activations increase until the hip flexion velocity reduces
271 to zero. At this point, the trunk is maximally flexed, phase 2 comes to an end. The knee joint extends
272 only slightly during phase 2. The peak VAS, GMAX and HAMS muscle activations occur during phase 2.
273 During phase 3, the activation of GMAX, HAMS, and VAS muscles slowly taper off as smaller forces are
274 required to continue standing up since an increasing fraction of body weight is borne by bone alignment.
275 These patterns lead to the extension of both the hip and knee joints until the standing posture is achieved.
276 At the end of phase 3, increased activation is observed in ILPSO, RF, and TA muscles to stop the hip, knee
277 and ankle joints from extending past the upright posture. Also, during the latter half of phase 3, the body's
278 COM reaches the feet support polygon. The SOL muscles see almost negligible activation; however, it
279 produces significant passive fiber forces during the first two phases and a significant part of the third phase.
280 Significant TA muscle activations are present during all three phases. These activations produce the force
281 needed to balance the counteracting SOL and GAS muscle forces.

282 The joint angle trajectories of 0% strength deficits are contrasted against those observed experimentally
283 for a healthy adult in Figure 6 (B). The general shape of the hip and knee joint angle trajectories matches
284 those of experiments. The discrepancies in the joint angle trajectories primarily result from the different
285 initial postures (Figure 5). The mean initial posture from experiments requires the lumbar joint extension
286 from -30° to nearly 0° . Our model did not include lumbar joint actuation for the reasons of modelling
287 simplification. The initial posture was modified to compensate for the non-actuated lumbar joint by moving
288 the model slightly forward and locking the lumbar joint with 10° of flexion.

289 The muscle activation patterns of the 0% strength deficit model are compared to those of experiments in
290 Figure 7. The general shape of activation patterns for the STS critical muscles, i.e., GMAX, HAMS and
291 VAS, matches the experiments' results. The higher activation of VAS than experiments during the first half
292 of phase 1 is potentially due to cost term ϕ_2 . Muscle RF features higher activation during STS initiation as
293 the model did not feature trunk muscles. The higher activation of TA than experiments is potentially due to
294 the passive fiber forces induced in SOL muscle due to initial posture. Experimental data features a small
295 peak in the TA, GAS and SOL muscle activations during phase 2. This peak is absent in the generated
296 STS. The experimental data did not include EMG signal for ILPSO muscle. The peak activations of all the
297 muscles except RF and TA are within the two standard deviations of the peaks observed experimentally.

298 The seat and feet contact forces trajectories of the 0% strength deficit model's STS transition are
299 compared to the experimental observations in Figure 10. The lower seat-pan forces than experiments are
300 most potentially because of the point on point constraint-based formulation. The flattening in the peak
301 feet forces for simulation is because of the cost term ϕ_{10} . Also, the seat-off in simulation occurs earlier
302 than in the experiments. It is potentially because of reduced horizontal momentum required due to initial
303 posture adjustment and the kinematic constraint-based seat force formulation, making it easier to develop
304 horizontal momentum.

305 3.2 STS Adaptation and Failure

306 With strength deficits, the STS duration and the peak VAS, GMAX, RF, ILPSO and TA muscle activations
307 increase (Table 4 and Figure 11). The peak HAMS muscle activation increases with strength deficits up to
308 40% strength deficit and then decreases for the 60% strength deficit. The peak VAS muscle activation is
309 higher than that of GMAX muscle up to 40% strength deficit and is equal for the 60% strength deficit. The
310 decrease in the peak HAMS muscle activation for the 60% strength deficit model's STS trajectory is to

311 alleviate the saturated antagonistic VAS muscle across the knee joint. It is evident from the contribution of
312 HAMS muscle to peak resultant knee torques dropping from -112.17% for the 40% strength deficit to
313 -30.99% for the 60% strength deficit. The reduced HAMS muscle activation saturates the GMAX muscle
314 as they work together to control the hip flexion. It is demonstrated by the contributions of HAMS muscle
315 to the peak resultant hip torques dropping from 70.26% for the 40% strength deficit to 54.7% for the 60%
316 strength deficit. Also, a reduction in the peaks of COM velocity, ground reaction forces, and GMAX,
317 HAMS and VAS muscle forces is observed from the 40% strength deficit to 60% strength deficit. Bobbert
318 et al. (2016) also observes that with strength deficits, the STS duration increases, while the peak COM
319 vertical velocity, peak GMAX, and VAS muscle forces decrease. However, Bobbert et al. (2016) does
320 not observe any significant reduction in HAMS muscle activation. It is potentially because Bobbert et al.
321 (2016) used the immediately prior solutions as the initial guess for the subsequent optimization. Besides
322 STS duration and peak muscle activation, we do not observe consistent trends between the 0% strength
323 deficit to 40% strength deficit STS trajectory. It is most potentially because the optimization converged to a
324 different local optimum for each model.

325 The optimization framework failed to generate the STS transition for the 80% strength deficit model. We
326 suspected the GMAX or the VAS muscle to be responsible for this failure as they were getting saturated for
327 the 60% strength deficit model's STS trajectory (Figure 11). We tracked the 60% strength deficit model's
328 successful STS trajectory using the OpenSim CMC Tool and the 80% strength deficit model aided by one
329 of two different reserve actuators setups. In the first setup, the optimal torque, i.e., torques generated per
330 unit control effort, for the hip and knee torque actuators were 100Nm and 1Nm respectively, while for the
331 second setup, they were 1Nm and 100Nm . The first setup favored the utilization of the hip reserve actuator,
332 while the second setup favored the utilization of the knee reserve actuator. The first setup's motion-tracking
333 features a peak torque of -19.81Nm by the knee reserve actuator and increased activation of both VAS
334 and RF muscles. The second setup-based motion-tracking features a peak torque of -12.05Nm by the hip
335 reserve actuator and increased HAMS and GMAX activations. The lower magnitude of reserve actuator
336 in the second setup suggests that the STS failure occurred because of VAS muscle weakness. Also, the
337 observation that peak VAS muscle activation is greater than or equal to that of GMAX muscle supports this
338 hypothesis.

339 3.3 Externally Assisted STS Transition

340 It was observed in the last subsection that assisting the musculoskeletal model primarily at the hip joint
341 leads to increased RF muscle activation, while assisting it primarily at the knee joint leads to increased
342 HAMS muscle activation. As STS transition is performed several times a day, assisting only at the hip or
343 the knee joint will lead to the RF or the HAMS muscle contracture. As both the muscles cross the hip joint,
344 their contracture has a high potential to cause back pain issues. Thus the external assistance was introduced
345 at the torso COM in the 80% strength deficit model. Also, assisting the model at the torso center of mass is
346 a good approximation for assisting a human at the underarms area. The underarms area is easily graspable,
347 and assistance using it helps simplify the design of probable STS assistance devices.

348 Physical assistance can help maintain or recover lower extremity strength when provided in an assist-
349 as-needed manner. Thus while generating the assisted STS trajectories, the over-utilization of external
350 assistance was penalized (Equation 6). Figure 12 shows the body postures, the assistance forces, and
351 muscle activation for the externally assisted 80% strength deficit model's STS trajectory. The trajectory
352 features utilization of external assistance when the VAS and GMAX muscle starts getting saturated, i.e., the
353 model only uses external assistance when needed. The peak magnitudes of external assistance's vertical and

354 horizontal components are 36.50% and 44.51% of body weight, respectively. The STS trajectory features
355 reduced peaks of com velocities, net hip and knee joint torques and the VAS, GMAX, and HAMS muscle
356 forces. The seat-off takes place with the torso in a more upright posture than unassisted models.

4 DISCUSSION

357 This paper presented and analyzed the sit-to-stand (STS) trajectories generated using an open-loop single
358 shooting optimization and musculoskeletal models with different strength deficits. The strength deficits
359 were introduced by simultaneously scaling the maximum isometric strength of all the muscles in steps of
360 20%. The optimization could successfully generate STS trajectories for models with up to 60% strength
361 deficits. The muscle activation patterns for the 0% strength deficit model agree reasonably with the
362 experimental observations for a healthy adult. A reduction in the peak HAMS muscle activation is observed
363 when the VAS muscle gets saturated due to the strength deficits. The reduced HAMS muscle activation
364 led to increased GMAX muscle activation. The motion-tracking results were used to suggest the VAS
365 muscle weakness to be responsible for optimization's failure to generate STS trajectories using the 80%
366 strength deficit model. The motion tracking results were also used to motivate the introduction of external
367 assistance at torso centre of mass. Optimization generated successful STS trajectories for the externally
368 assisted 80% strength deficit model. The optimal trajectory featured the utilization of external assistance in
369 an assist-as-needed manner. After clinical validation, the reduced ratio of peak HAMS to GMAX muscle
370 weakness might be used to plan intervention. We have made the source code for optimization public to
371 speed up the design of future assist-as-needed STS care devices. Finally, the findings of this study should
372 be observed with caution as it they have many inherent assumptions. The most significant among them are
373 discussed in the following few paragraphs, followed by our probable future research directions.

374 Many experimental studies report that the elderly follow a stabilization strategy in which they move the
375 centre of mass over the feet support polygon before getting off the chair. The stabilization strategy, like
376 the mean initial posture of our experiments, requires significant lumbar motion. Also, the COM lies just
377 1.15cm inside the feet support polygon for the maximum amount of trunk flexion with chair contact. Thus
378 the elimination of the lumbar joint and the feet-ground relative degree of freedom, even though also made
379 by Pandy et al. (1995), Bobbert et al. (2016), and Yokota et al. (2016), might be oversimplifications for
380 predicting STS trajectories of the elderly adults.

381 The strength deficits were introduced by simultaneously scaling the maximum isometric strength of all
382 the muscles. Bobbert et al. (2016) and Yokota et al. (2016) also introduced strength deficits in a similar
383 manner. However, the strengths of all the muscles do not deteriorate by the same ratio. Also, scaling
384 the maximum isometric forces is not the only way to introduce strength deficits. For example, the peak
385 muscle activations could have been limited to the same effect. Thus the strength deficit modelling should
386 be investigated for more accurate predictions.

387 We assumed a sagittal plane of symmetry. However, it has been shown that even for healthy adults, one
388 leg is usually more dominant than the other. Also, significant asymmetries may arise when one of the upper
389 extremities grabs surfaces for assistance. Thus, the optimization framework needs to be extended to use
390 the 3D musculoskeletal model to generate more realistic assisted and unassisted STS trajectories. Other
391 musculoskeletal model-related critical assumptions that must be validated are simplifying muscle groups to
392 single musculotendon units and the control level decoupling of muscles.

393 We assumed perfect coordination between the musculoskeletal model and the external assistance, which
394 led to an optimal trajectory with 1.11sec STS duration. The optimization framework should be extended to

395 include sensory noise and delay in external assistance formulation to synthesize realistically replicable
396 STS trajectories. The maximum simulation duration was limited to 1.6sec and might have prevented the
397 search of successful STS trajectories. Also, the chair height and the initial posture heavily influence the
398 STS transitions, and the results of this study are a function of them.

399 The cost function used in this study is not unique in its capability to engender STS. Further, even for the
400 selected cost function, the relative weights of the different cost terms should have been chosen using inverse
401 optimal control. The relative weights were selected using trial and error because of the computationally
402 demanding nature of the optimization. The generated STS trajectories are local optimal solutions of
403 nonlinear non-convex optimizations. The optimization's failure to generate STS using the 80% strength
404 deficit model might have been due to the unsuccessful search rather than muscle saturation.

405 In the future, we plan to design a kinematic events-based closed-loop STS controller to enable the
406 modelling of reduction in balance capabilities. We also plan to investigate the torque and muscle actuated
407 lumbar joint models for STS trajectories with more accurate joint kinematics and dynamics. Finally, we
408 intend to extend the optimization framework to include sensory noise and delay for the more realistic
409 models of assist-as-needed STS care devices.

5 AUTHOR CONTRIBUTIONS

410 Conceptualization: VK, TY, and TS; Methodology: VK; Software: VK; Data Analysis: VK; Validation:
411 TS; Writing—original draft preparation: VK; Writing—review and editing: VK, TY, and TS; Funding
412 acquisition: TS; Resources: TY and TS; Supervision: TS

6 ACKNOWLEDGEMENT

413 We would like to thank Dr. Tamei Tomoya of Kobe University for sharing the experimental data.

7 DATA AVAILABILITY STATEMENT

414 The optimization source code and the results from this study are available at <https://github.com/ShibataLab/PredictiveSTS>.
415

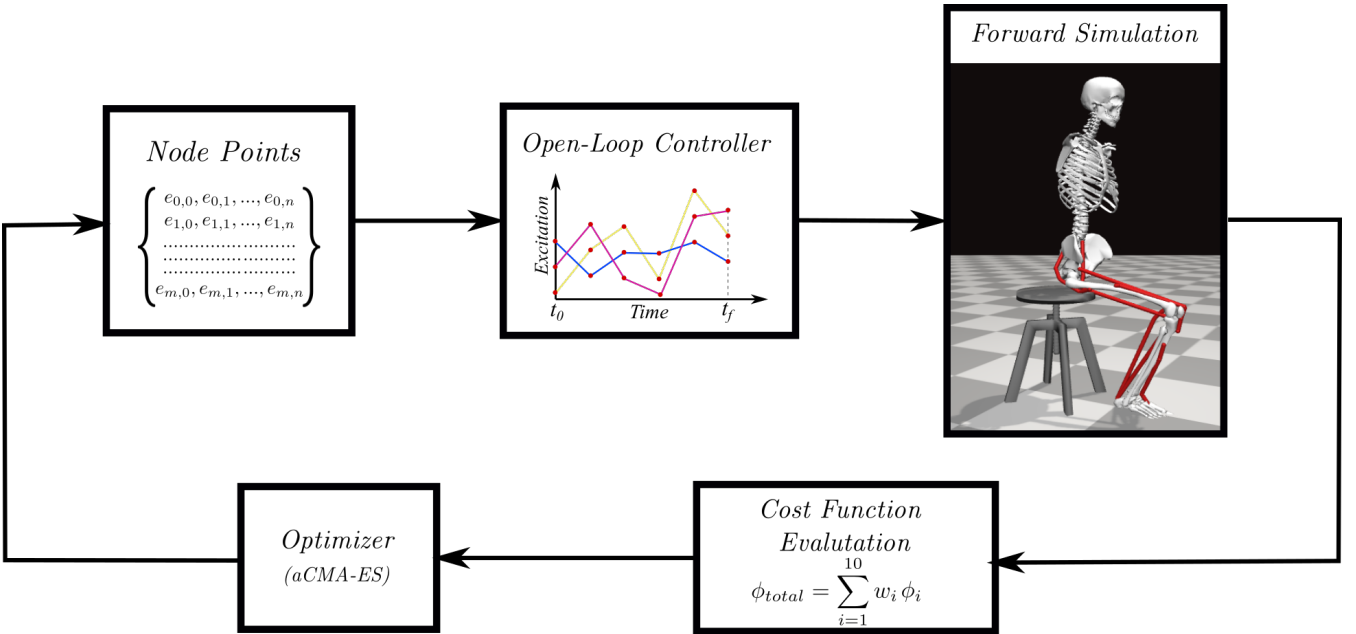


Figure 1. Overview of single shooting optimization framework. The red dots in the open-loop controller represents the node points obtained from the discretization of excitation trajectories.

Muscle	Acronym	Maximum Isometric Strength (N)
Iliopsoas	ILPSO	2697.3
Gluteus maximus	GMAX	3337.6
Biarticular Rectus Femoris	RF	2191.7
Biarticular Hamstrings	HAMS	4105.5
Vasti	VAS	9594.0
Biarticular Gastrocnemius	GAS	4690.6
Soleus	SOL	7925.0
Tibialis Anterior	TA	2116.8

Table 1. Muscles included in the model, their acronyms and their respective maximum isometric strengths for the 0% strength deficit model.

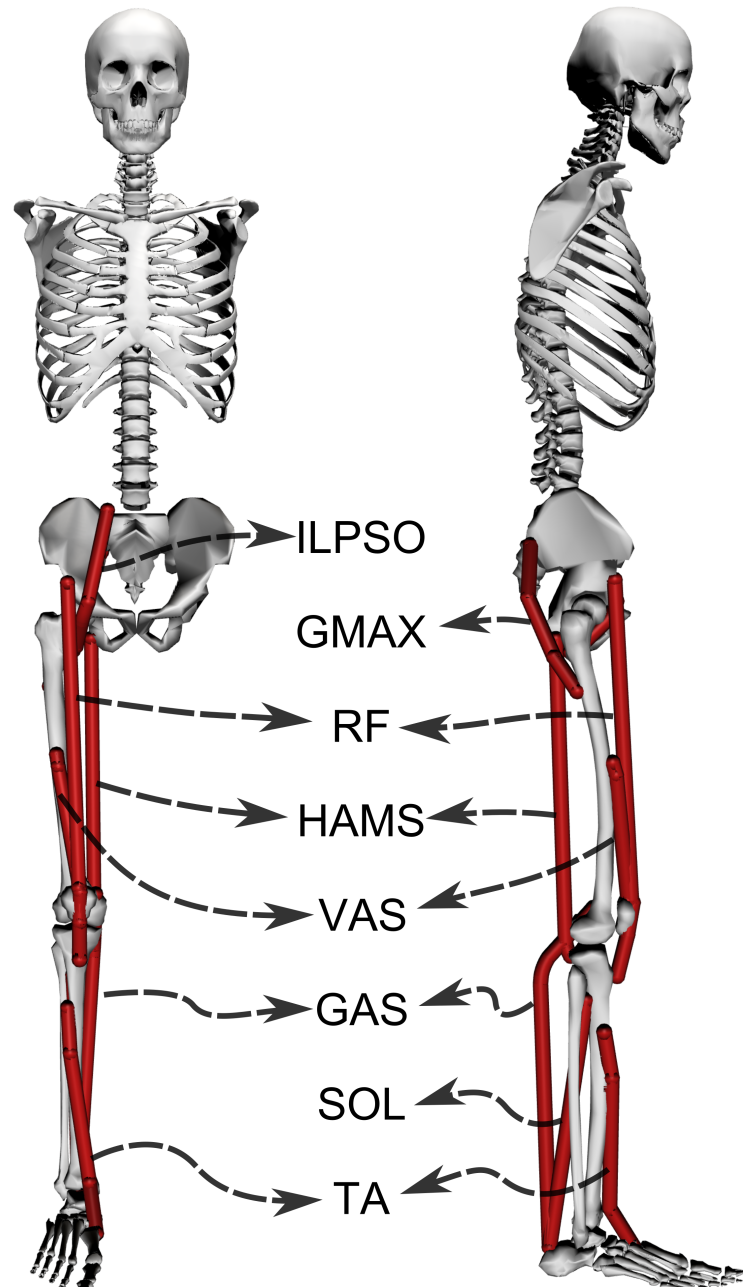


Figure 2. A planar musculoskeletal model for sit-to-stand. The model's musculotendon actuators (red lines) represents the major uniarticular and biarticular muscle groups that drive the sit-to-stand motion in the sagittal plane, i.e., iliopsoas (ILPSO), gluteus maximus (GMAX), biarticular rectus femoris (RF), biarticular hamstrings (HAMS), vasti (VAS), gastrocnemius (GAS), soleus (SOL), and tibialis anterior (TA). The model has three degrees of freedom distributed at the hip, knee and ankle joints.

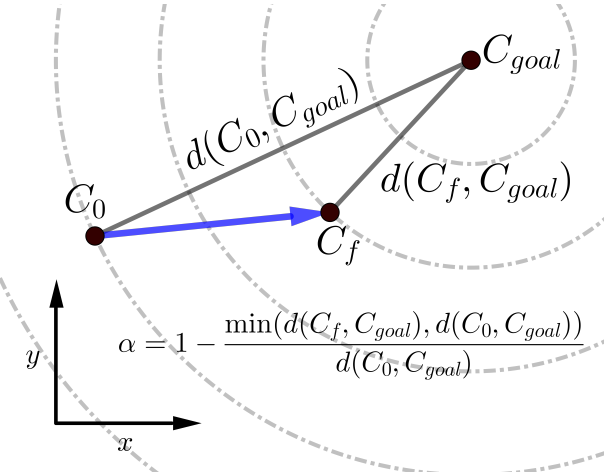


Figure 3. Scalar α , used within the cost expressions, represents the percentage of STS completion and ranges between 0 to 1. The dashed circles show the states that are equidistant from the C_{goal} .

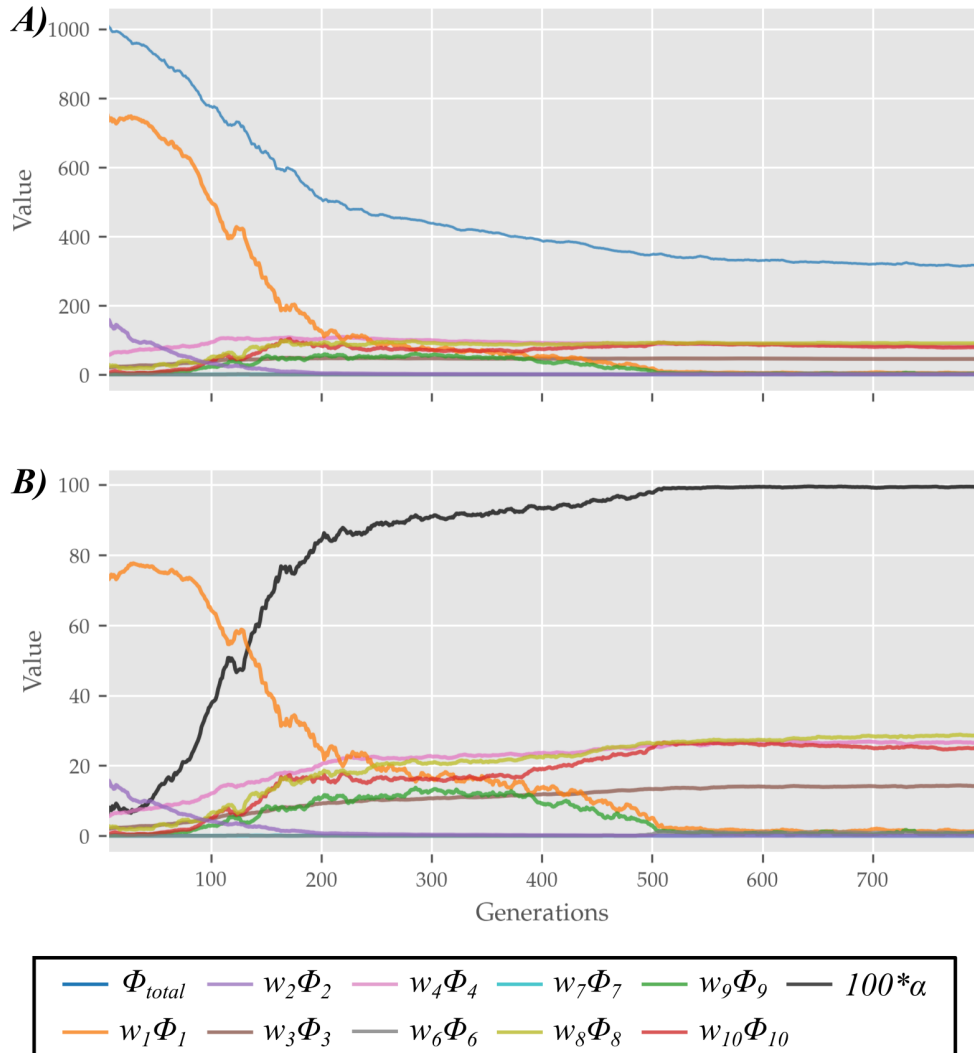


Figure 4. Evolution of different costs (**A**) and their relative contributions to the total cost (**B**) for the best candidates observed during trajectory optimization using the 0% strength deficit model. The costs were smoothed using a rolling average of 10 generations for this plot.

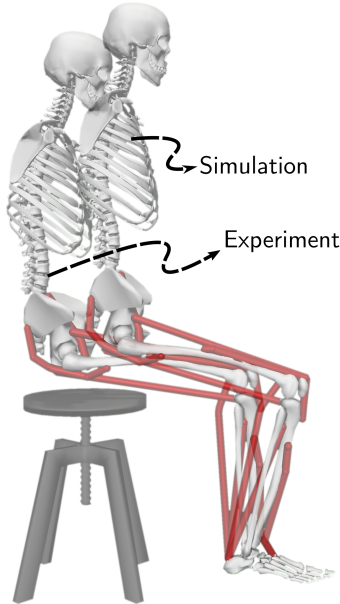


Figure 5. The initial posture used to generate STS trajectories and the mean initial posture observed during experiments. The model was moved slightly forward for simulation to compensate for its non-actuated lumbar joint.

Table 2. List of symbols.

Variable	Description
t	time
$\dots(t)$	Value of a expression .. at time t
$.. $	The absolute value expression ..
t_0	Simulation start time
t_f	Simulation final time
t_{max}	Upper limit of t_f
t_{SR}	Time of seat release
C_0	Center of mass at t_0
C_f	Center of mass at t_f
C_{goal}	Center of mass for standing posture
$d(C_1, C_2)$	Euclidean distance between center of mass positions at t_1 and t_2
α	% Sit to stand completion
$F_{chair,y}$	y component of constraint force applied by the chair on the femur head
τ	Time constant
a_i	Activation of actuator i
$ F_{Assist} $	Magnitude of external assistance
$T_{n,limit}$	Torque generated by the torsional limit spring at the n^{th} joint
$F_{feet,n}$	Component of force applied along n direction by the ground on the feet
ZMP_x	x coordinate of feet force zero moment point
$\dot{\theta}_j$	Velocity of joint j
$Feet_x$	x coordinate of the mid point between heel and toes
mg	Weight of musculoskeletal model

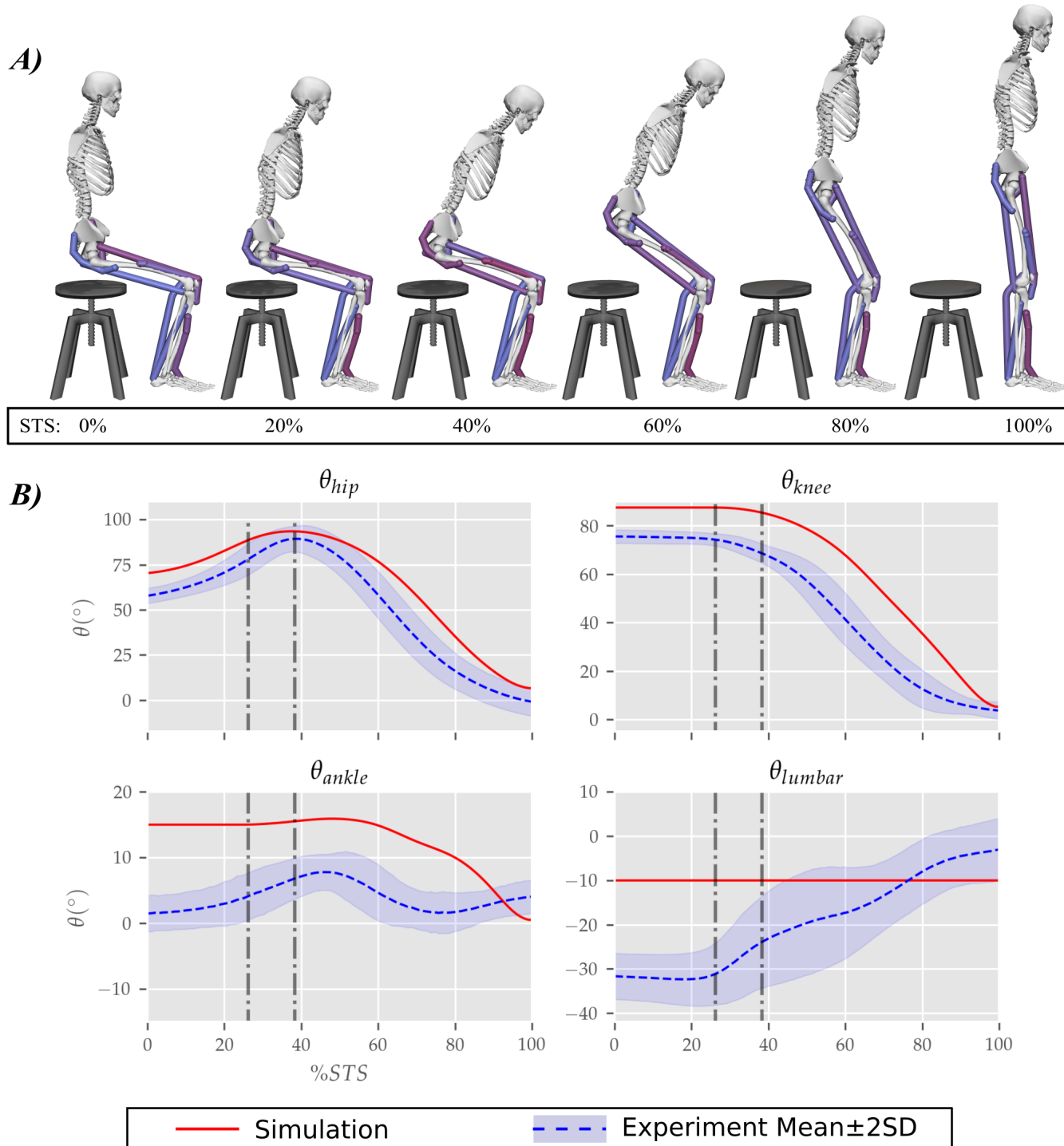


Figure 6. (A) Different postures observed during the STS transition of the 0% strength deficit model and the comparison of associated joint angle trajectories against experimental recordings (B). The first vertical dotted line marks the point when the model lost contact with the chair, and the second vertical dotted line marks the posture with maximum hip flexion.

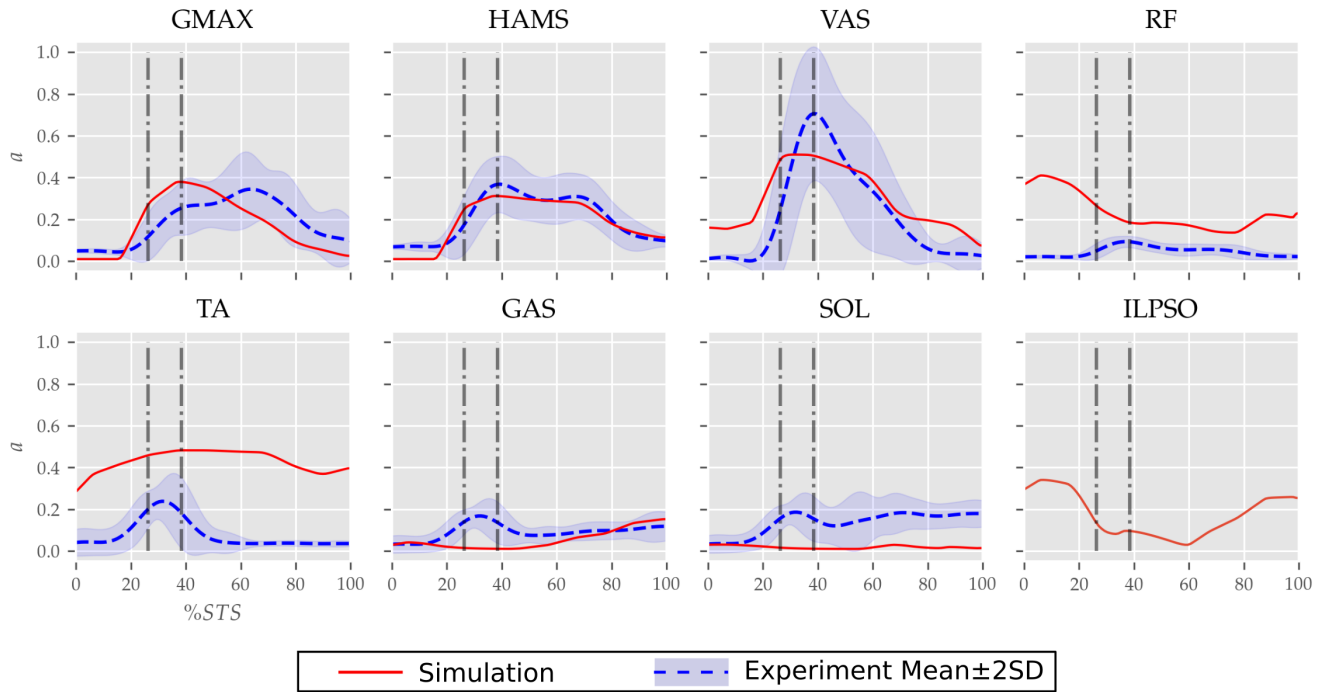


Figure 7. Muscle activation trajectories associated with the 0% strength deficit model's STS trajectory and those recorded experimentally.

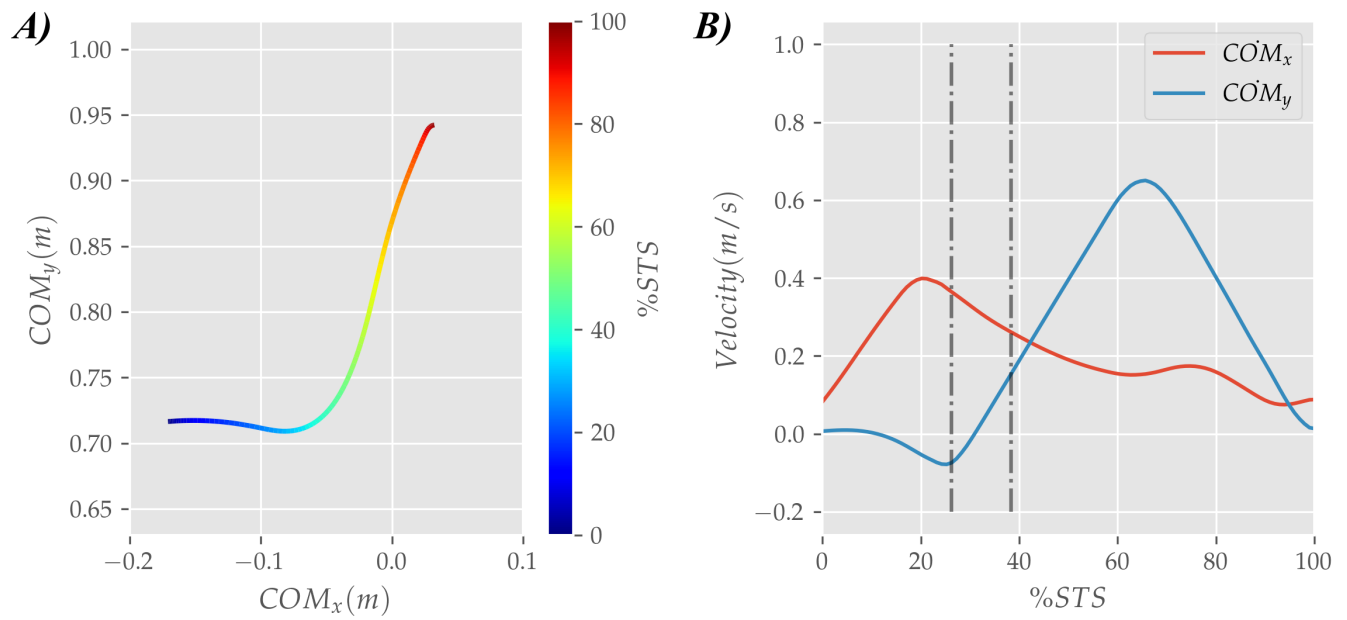


Figure 8. Evolution of COM position (**A**) and velocity (**B**) observed for the STS trajectory of 0% strength deficit model.

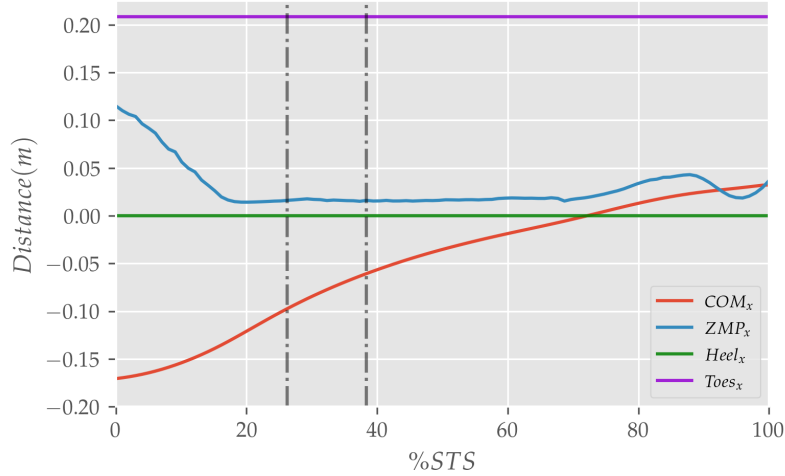


Figure 9. The zero moment point (feet forces) and the body's COM trajectories from the 0% strength deficit model's STS.

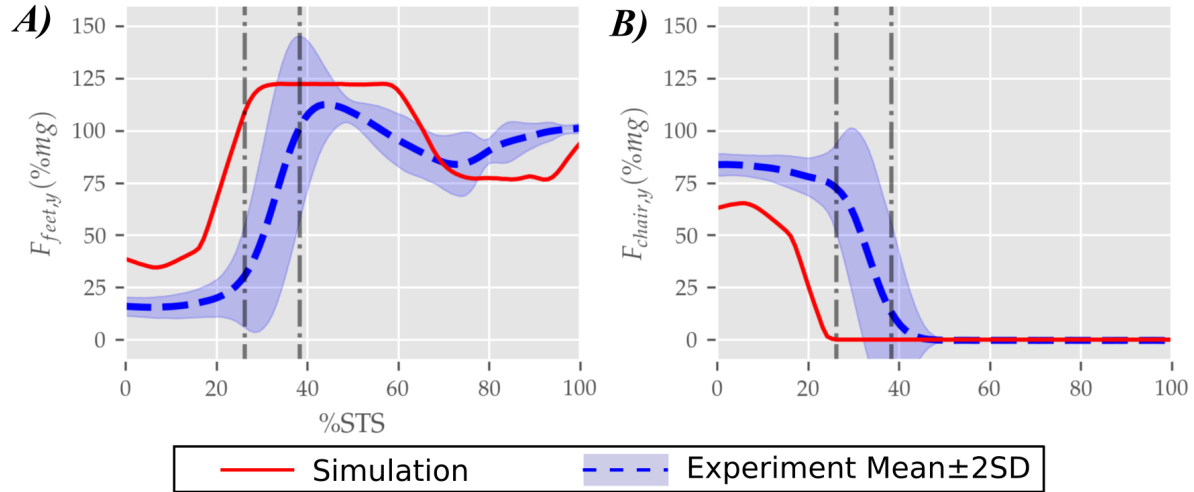


Figure 10. Feet (A) and seat contact forces (B) observed during the STS trajectory of the 0% strength deficit model and the experiments.

Table 3. Cost function hyperparameters.

Variable	Value
τ	$t_{max}/8$
w_1	800
w_2	1.2
w_3	175
w_4	70
w_5	5
w_6	10
w_7	0.1
w_8	1000
w_9	6
w_{10}	0.3

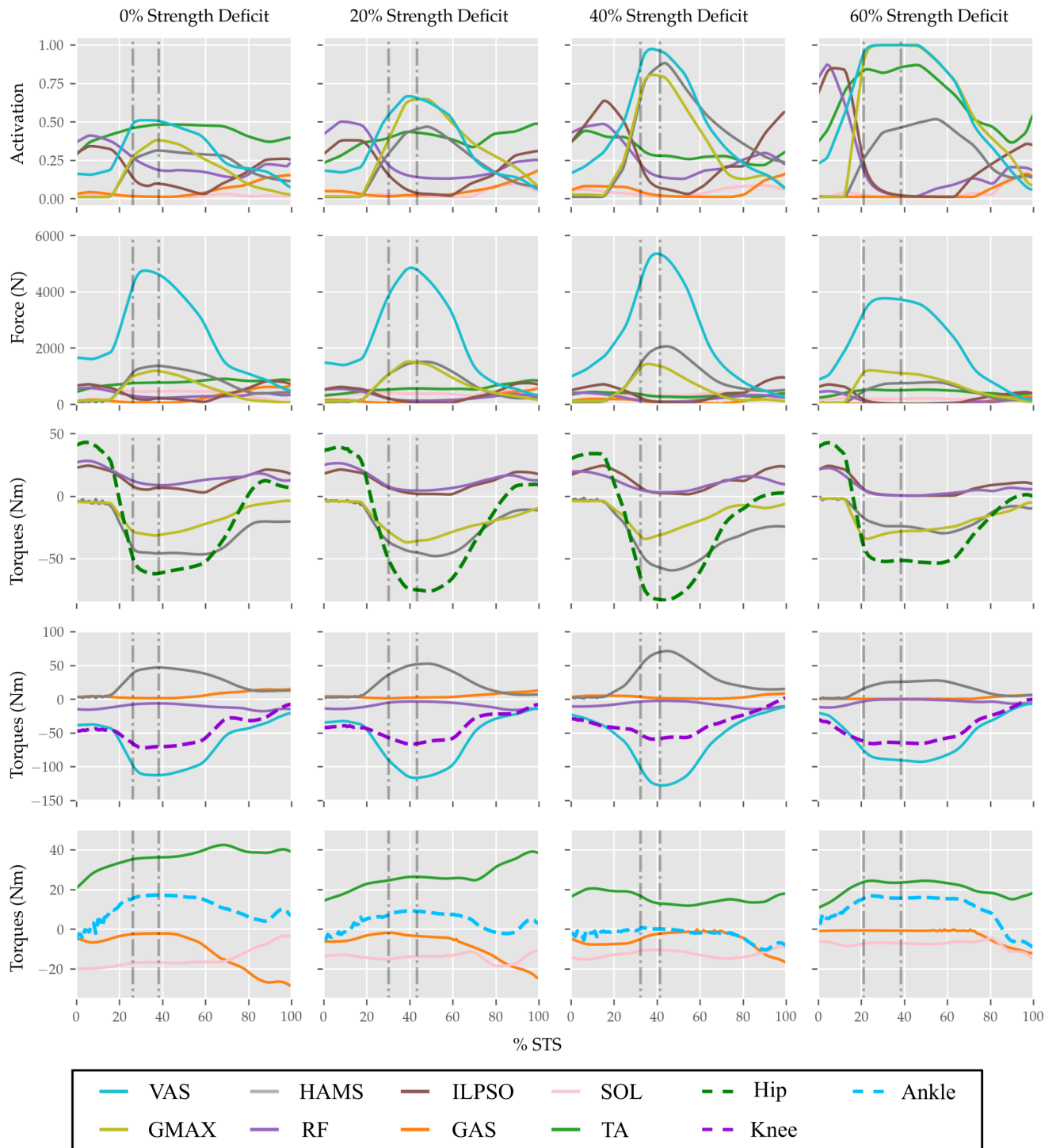


Figure 11. Muscle activations, muscle forces, and their respective contributions to the resultant joint torques from the STS trajectories of 0%, 20%, 40% and 60% strength deficit models.

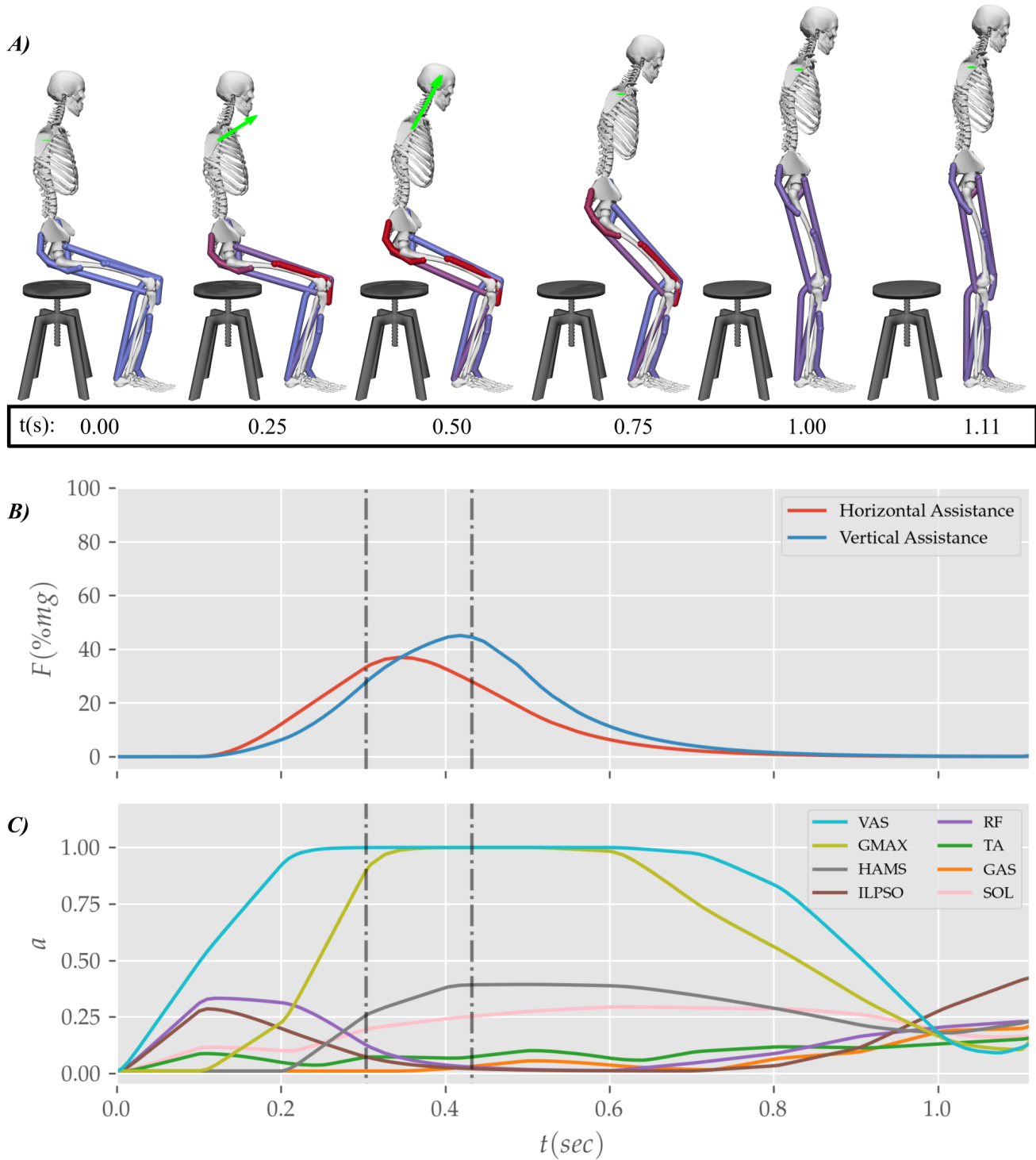


Figure 12. Postures (A) and the external assistance trajectories (B) from the STS transition of the externally assisted 80% strength deficit model. The green arrow in (A) represents the resultant external assistance force.

Table 4. Properties of the 0%, 20%, 40%, 60% and externally assisted 80% strength deficit model's STS trajectories. Rows 5, 6, 8 and 10 show contributions of muscles to peak resultant joint torques.

# Row	Property	0% Strength Deficit	20% Strength Deficit	40% Strength Deficit	60% Strength Deficit	80% Strength Deficit Assisted
1	STS duration (s)	1.14	1.23	1.33	1.47	1.11
2	Peak COM Horizontal Velocity (m/s)	0.40	0.42	0.42	0.39	0.43
3	Peak COM Vertical Velocity (m/s)	0.65	0.71	0.65	0.55	0.42
4	Peak Hip Torque (Nm)	-62.17	-76.10	-83.28	-53.58	-35.59
5	GMAX Peak Hip Torque (Nm)	-31.60	-35.12	-30.03	-26.17	-20.96
6	HAMS Peak Hip Torque (Nm)	-45.91	-47.15	-58.51	-29.31	-15.44
7	Peak Knee Torque (Nm)	-72.02	-66.73	-59.22	-65.86	-42.19
8	VAS Peak Knee Torque (Nm)	-111.26	-115.92	-125.02	-85.51	-42.36
9	HAMS Peak Knee Torque (Nm)	44.40	50.34	66.43	20.41	2.69
10	Peak VAS Force (N)	4754.10	4857.40	5355.19	3765.91	1907.14
11	Peak GMAX Force (N)	1194.27	1513.42	1437.11	1206.33	615.33
12	Peak HAMS Force (N)	1366.03	1505.99	2058.45	782.31	340.31

REFERENCES

- 416 Arnold, D. V. and Hansen, N. (2010). Active covariance matrix adaptation for the (1+ 1)-cma-es. In
417 *Proceedings of the 12th annual conference on Genetic and evolutionary computation*. 385–392
- 418 Bobbert, M. F., Kistemaker, D. A., Vaz, M. A., and Ackermann, M. (2016). Searching for strategies to
419 reduce the mechanical demands of the sit-to-stand task with a muscle-actuated optimal control model.
420 *Clinical Biomechanics* 37, 83–90
- 421 [Dataset] CMA-ES (2013). libcmaes. <https://github.com/CMA-ES/libcmaes>
- 422 Delp, S. L., Anderson, F. C., Arnold, A. S., Loan, P., Habib, A., John, C. T., et al. (2007). Opensim:
423 open-source software to create and analyze dynamic simulations of movement. *IEEE transactions on*
424 *biomedical engineering* 54, 1940–1950
- 425 Geravand, M., Korondi, P. Z., Werner, C., Hauer, K., and Peer, A. (2017). Human sit-to-stand transfer
426 modeling towards intuitive and biologically-inspired robot assistance. *Autonomous Robots* 41, 575–592
- 427 Hughes, M. A., Myers, B. S., and Schenkman, M. L. (1996). The role of strength in rising from a chair in
428 the functionally impaired elderly. *Journal of biomechanics* 29, 1509–1513
- 429 Lai, A. K., Arnold, A. S., and Wakeling, J. M. (2017). Why are antagonist muscles co-activated in my
430 simulation? a musculoskeletal model for analysing human locomotor tasks. *Annals of biomedical*
431 *engineering* 45, 2762–2774
- 432 Lao, B., Tamei, T., and Ikeda, K. (2019). Characterizing strategic contributions of physical therapy to
433 natural standing motion in the muscle synergy space. In *2019 41st Annual International Conference of*
434 *the IEEE Engineering in Medicine and Biology Society (EMBC)* (IEEE), 2311–2315
- 435 Lao, B., Tamei, T., and Ikeda, K. (2020). Data-efficient framework for personalized physiotherapy feedback.
436 *Frontiers in Computer Science* 2, 3
- 437 Lord, S. R., Murray, S. M., Chapman, K., Munro, B., and Tiedemann, A. (2002). Sit-to-stand performance
438 depends on sensation, speed, balance, and psychological status in addition to strength in older people.
439 *The Journals of Gerontology Series A: Biological Sciences and Medical Sciences* 57, M539–M543
- 440 Millard, M. (1999). First-order activation dynamics
- 441 Millington, P. J., Myklebust, B. M., and Shambes, G. M. (1992). Biomechanical analysis of the sit-to-stand
442 motion in elderly persons. *Archives of Physical Medicine and Rehabilitation* 73, 609–617
- 443 Mombaur, K. and Hoang, K.-L. H. (2017). How to best support sit to stand transfers of geriatric patients:
444 Motion optimization under external forces for the design of physical assistive devices. *Journal of*
445 *biomechanics* 58, 131–138
- 446 Norman-Gerum, V. and McPhee, J. (2018). Constrained dynamic optimization of sit-to-stand motion
447 driven by bézier curves. *Journal of biomechanical engineering* 140
- 448 Ong, C. F., Geijtenbeek, T., Hicks, J. L., and Delp, S. L. (2019). Predicting gait adaptations due to ankle
449 plantarflexor muscle weakness and contracture using physics-based musculoskeletal simulations. *PLoS*
450 *computational biology* 15, e1006993
- 451 Ozsoy, B. and Yang, J. (2021). Assisted spatial sit-to-stand prediction—part 2: Virtual injured elderly
452 individuals. *Journal of Computing and Information Science in Engineering* 21, 061009
- 453 Pandy, M., Garner, B., and Anderson, F. (1995). Optimal control of non-ballistic muscular movements: a
454 constraint-based performance criterion for rising from a chair. *Journal of Biomechanical Engineering*
455 117, 15
- 456 Sadeghi, M., Andani, M. E., Bahrami, F., and Parnianpour, M. (2013). Trajectory of human movement
457 during sit to stand: a new modeling approach based on movement decomposition and multi-phase cost
458 function. *Experimental brain research* 229, 221–234

- 459 Schenkman, M., Hughes, M. A., Samsa, G., and Studenski, S. (1996). The relative importance of strength
460 and balance in chair rise by functionally impaired older individuals. *Journal of the American Geriatrics
461 Society* 44, 1441–1446
- 462 Yang, J. and Ozsoy, B. (2020). Three dimensional unassisted sit-to-stand prediction for virtual healthy
463 young and elderly individuals. *Multibody System Dynamics* 49, 33–52
- 464 Yang, J. and Ozsoy, B. (2021). Assisted spatial sit-to-stand prediction-part 1: Virtual healthy elderly
465 individuals. *Journal of Computing and Information Science in Engineering* 21, 041002
- 466 Yokota, H., Ohshima, S., and Mizuno, N. (2016). Sit-to-stand motion analysis using multiobjective
467 genetic algorithm based on musculoskeletal model simulation. *IEEJ Journal of Industry Applications* 5,
468 236–244
- 469 Yoshioka, S., Nagano, A., Hay, D. C., and Fukashiro, S. (2012). The minimum required muscle force for a
470 sit-to-stand task. *Journal of biomechanics* 45, 699–705
- 471 Yoshioka, S., Nagano, A., Himeno, R., and Fukashiro, S. (2007). Computation of the kinematics and the
472 minimum peak joint moments of sit-to-stand movements. *Biomedical engineering online* 6, 1–14

Supplementary Material

1 SUPPLEMENTARY FIGURES

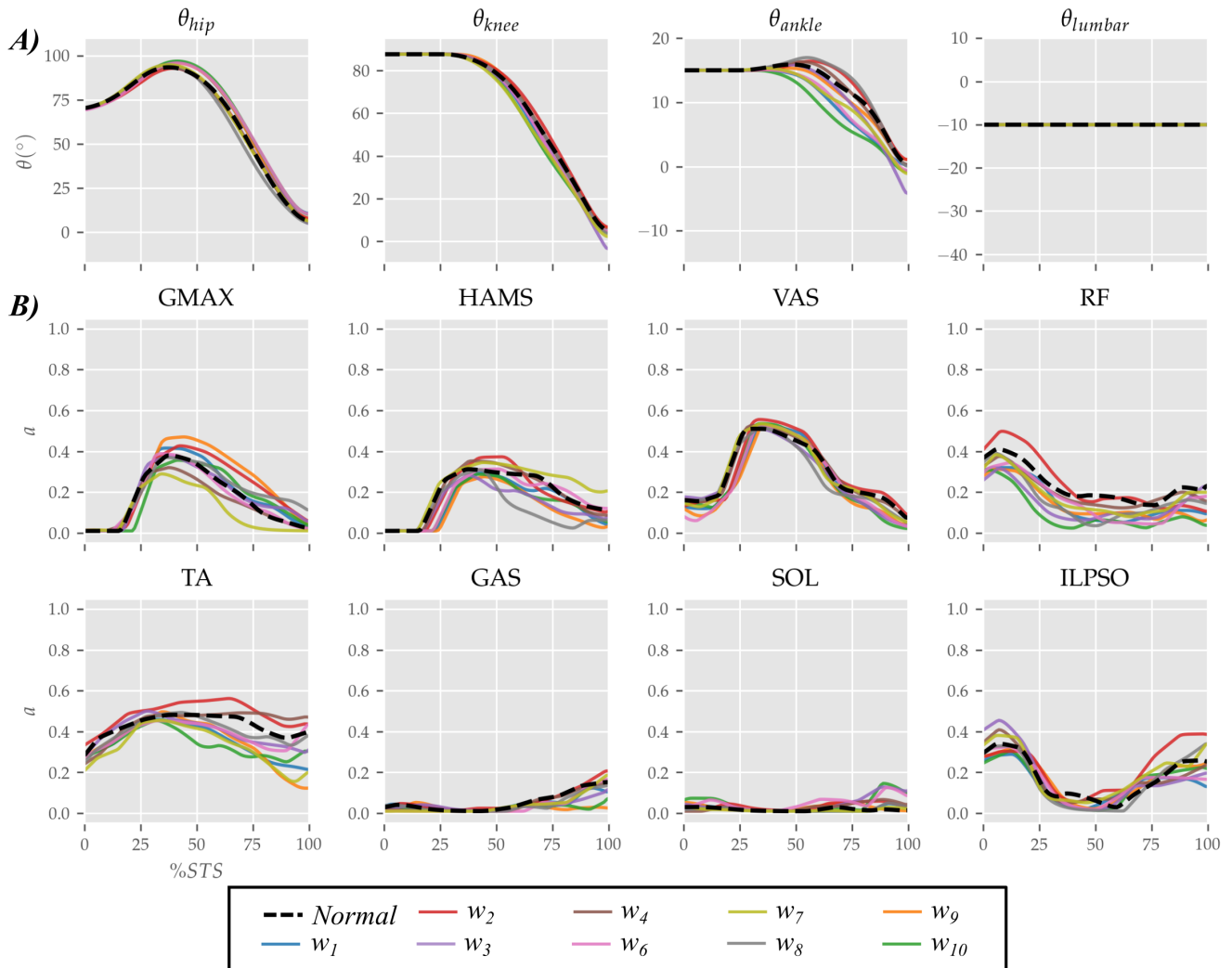


Figure S1. Joint angle (A) and muscle activation (B) trajectories obtained using the 0% strength deficit model with normal relative weights as listed in Table 3 and the relative weights increased individually by 10%. The resulting STS trajectories appear reasonably robust to relative weights.

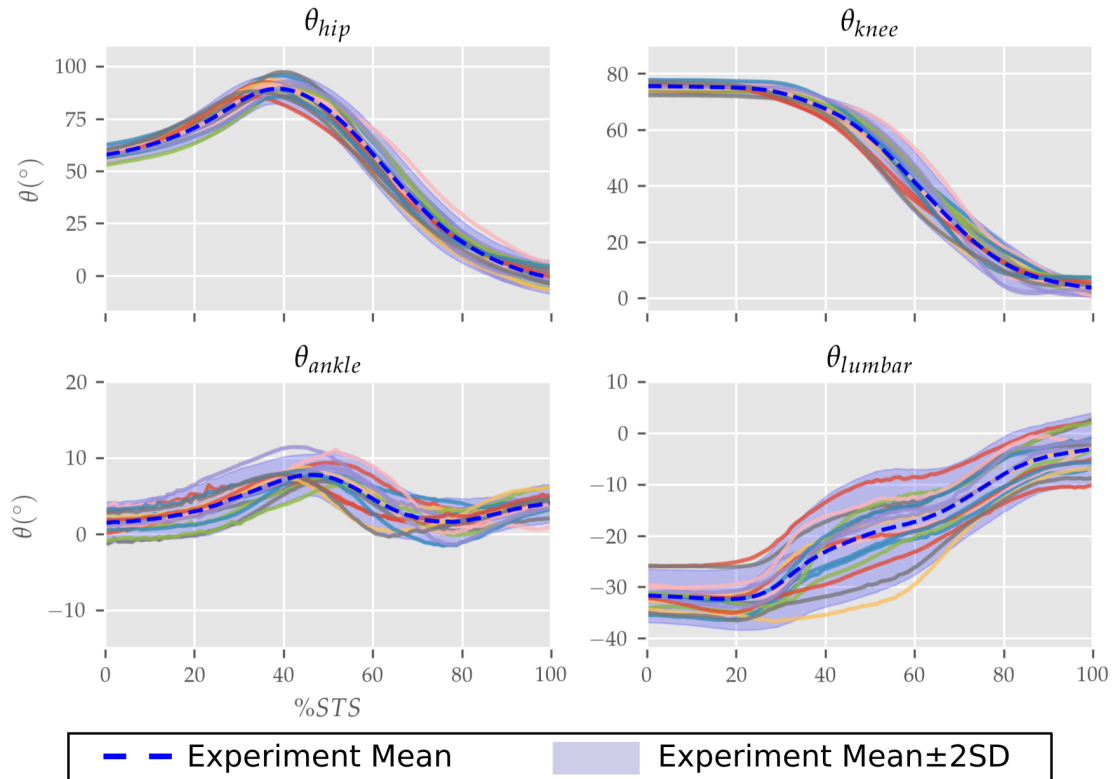


Figure S2. Joint angle trajectories from the experimental trials of the healthy adult. The beginning and the end of STS were defined as the points when hip flexion and hip extensions velocities smoothed with a rolling window of 0.1s grew respectively higher or lower than $20^\circ/\text{s}$.

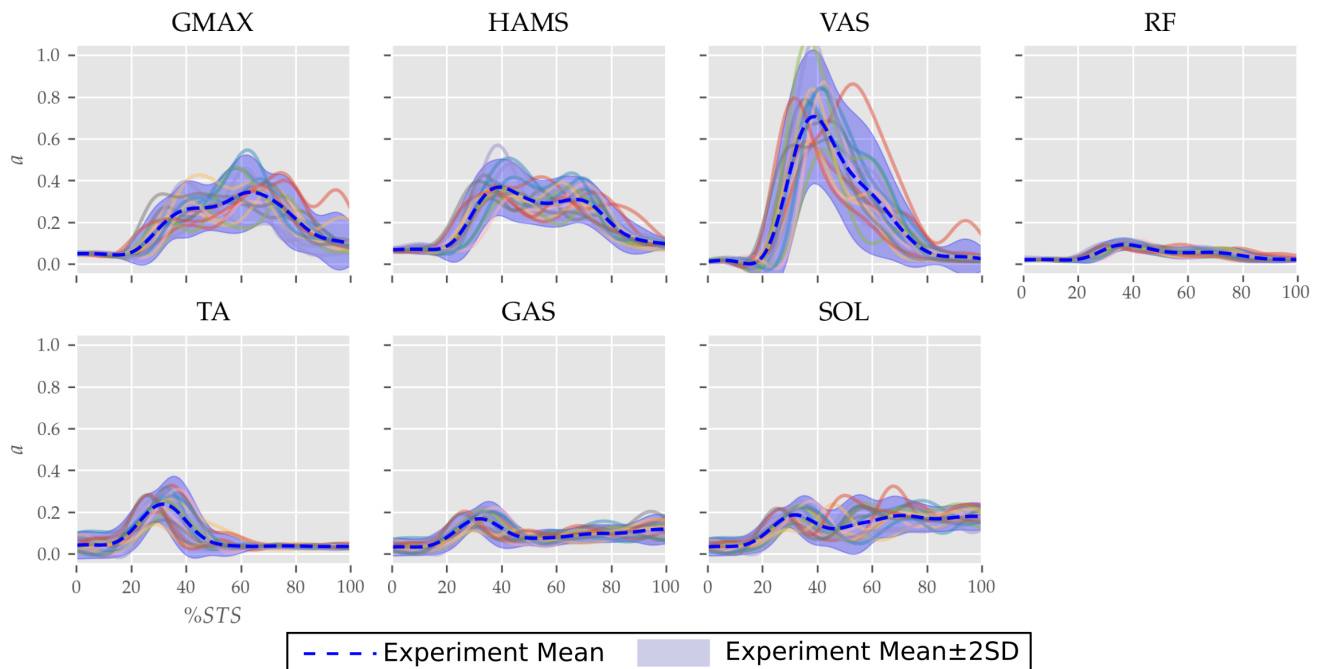


Figure S3. Muscle activation trajectories from the experimental trials of the healthy adult.

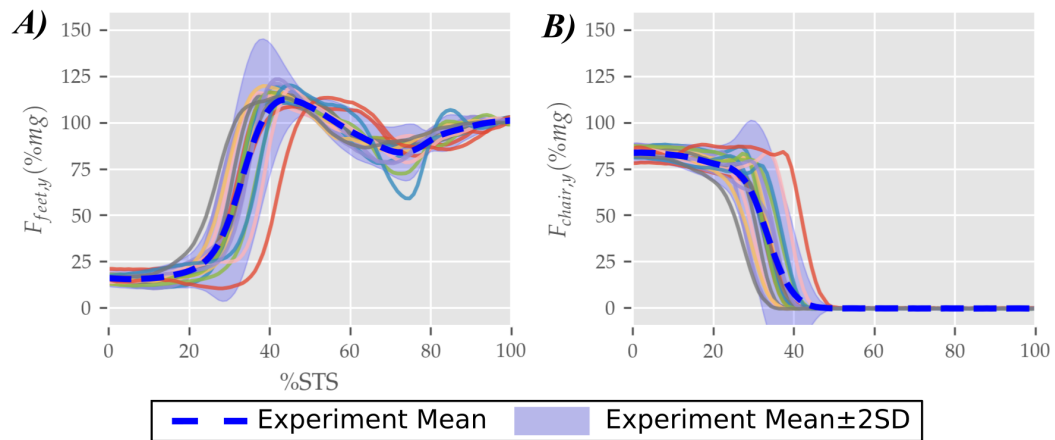


Figure S4. Seat and ground reaction force trajectories from the experimental trials of the healthy adult.